Finite element analysis of frequency- and temperature-dependent hybrid active-passive vibration damping

Marcelo A. Trindade — Ayech Benjeddou — Roger Ohayon

Structural Mechanics and Coupled Systems Laboratory
Conservatoire National des Arts et Métiers, 2, rue Conté, 75003 Paris
{trindade, benjedou, ohayon}@cnam.fr

RÉSUMÉ. *Un nouvel élément fini est formulé et utilisé pour analyser des poutres sandwich à peaux piézoélectriques stratifiées. L'amortissement viscoélastique du coeur est modélisé par trois méthodes, à savoir Golla-Hughes-McTavish, champs de déplacements non élastiques et une version itérative de la méthode des énergies modales. Puisque les deux premiers modèles augmentent beaucoup la dimension du système, on propose une réduction modale. Les modèles réduits sont ensuite appliqués pour l'analyse de l'amortissement par couche de contrainte active d'une poutre encastrée-libre, en utilisant un algorithme de contrôle optimal contraint. En outre, l'effet des variations de la température sur la performance de l'amortissement est étudié.*

ABSTRACT. *A new finite element is formulated and used for the analysis of sandwich damped beams with laminate piezoelectric faces. The viscoelastic damping of the core is accounted for using three models, namely Golla-Hughes-McTavish, Anelastic Displacement Fields and Iterative Modal Strain Energy. Since the first two models increase much the system dimension, a modal reduction is proposed. The reduced models are then applied to the analysis of active constrained layer damping treatments of a cantilever beam, using a constrained input optimal control algorithm. Furthermore, the effect of temperature variations on the control performance is studied.*

MOTS-CLÉS : *Matériaux viscoélastiques, matériaux piézoélectriques, amortissement hybride actif-passif, contrôle de vibrations, élément fini.*

KEY WORDS : *Viscoelastic materials, piezoelectric materials, hybrid active-passive damping, vibration control, finite element.*

1. Introduction

Since the beginning of the nineties, there has been an increasing interest in hybrid active-passive damping technologies, using piezoelectric and viscoelastic materials in a single treatment. This is mainly due to the complementarities of such damping treatments. Passive damping is known to be robust and reliable but performance is generally limited by weight and dimension constraints. While active control allows to overdamp some selected modes with very small actuators. One such hybrid damping treatment is obtained by replacing, or augmenting, the constraining layer of a passive constrained layer damping (PCLD) treatment by a piezoelectric actuator. This mechanism, the so-called active constrained layer damping (ACLD), allows to increase actively the viscoelastic layer shear strain and, consequently, the energy dissipation. Review on active constrained layer damping treatments can be found in [BEN 99a, INM 97]. The performance of such a treatment is the result of a compromise between increase of viscoelastic dissipation and loss of actuation transmissibility. Thus, it is highly dependent on viscoelastic material stiffness and damping properties, which depend strongly on temperature and frequency. Hence, modeling these dependences is very important for the control synthesis. Lesieutre and his co-workers [LES 95, LES 96b] and Hughes and his co-workers [GOL 85, MCT 93] proposed the so-called Anelastic Displacement Fields (ADF) and Golla-Hughes-McTavish (GHM) models, which are based on the introduction of internal variables to account for viscoelastic relaxation and, thus, damping behavior. They were shown to be superior to the Modal Strain Energy (MSE) method proposed in [JOH 81], although they are more complex and much increase the system dimension, so that a modal reduction is required. Both ADF and GHM models parameters are evaluated from materials properties at a given constant temperature. Lesieutre and Govindswamy [LES 96a] presented an extension of the ADF model capable of predicting self-heating and temperature-dependence of viscoelastic materials in simple shear, however leading to nonlinear equations of motion. GHM model was applied to ACLD treatments mainly by Inman and his students [PAR 99], who also studied its model reduction, and Liao and Wang [LIA 97]. On the other hand, Friswell and Inman [FRI 98] proposed the use of an iterative version of the MSE method, in conjunction with a complex-based model reduction, as an alternative to internal variables approach. They also presented the effect of temperature variations of viscoelastic material on the control performance. Also to account for viscoelastic damping, Plouin and Balmès [PLO 98] proposed an augmented real-based modal reduction technique, however the system dimension is doubled.

Piezoelectric three-layer sandwich beam finite element models were presented in previous works [BEN 97, BEN 99b]. They are extended here to treat sandwich damped beams with laminate piezoelectric faces and viscoelastic core. Finite element implementation of ADF, GHM and MSE viscoelastic models is also given. A model reduction of the ADF and GHM augmented systems is proposed. Then, the resulting reduced models are applied to the analysis of ACLD treatments of a cantilever beam,

using a constrained input optimal control algorithm. Finally, the effect of temperature variations on the control performance is studied and a temperature-dependent control synthesis is analyzed.

2. Finite element formulation

A sandwich beam made of viscoelastic core and laminate, elastic or piezoelectric, faces is considered. The latter are modeled using classical laminate theory, whereas the face/core/face system is modeled using classical three-layer sandwich theory and the kinematics description proposed in [BEN 99b]. All layers are supposed perfectly bonded, in plane stress state and having the same transverse displacement. The deformation of the face sheets obeys Euler-Bernoulli theory, whereas Timoshenko one is used for the core. Piezoelectric laminaes of the faces are poled through-thickness and subjected to transverse electrical fields. Other non-piezoelectric layers are assumed insulated. The parameters L, b and h denote length, width and thickness constants and the subscripts a_j, b_j and c relate to the j-th laminae of the upper a and lower b faces and to the core, respectively.

2.1. *Displacement and strain interpolations*

Assuming linear through-thickness axial displacements for the multilayer faces and core, and enforcing continuity conditions between layers, one may write the following axial displacements expressions

$$\breve{u}_i = u_i + (z - z_i)\beta_i \; ; \; \breve{w}_i = w \; ; \quad i = a,b,c \qquad [1]$$

where

$$u_k = \bar{u} \pm \frac{\tilde{u}}{2} \; ; \; \beta_k = -w' \; ; \; k = a(+),b(-) \; ; \; u_c = \bar{u} + dw' \; ; \; \beta_c = \frac{\tilde{u}}{h_c} + \lambda w'$$

and

$$d = \tfrac{h_a - h_b}{4} \; ; \quad \lambda = \tfrac{h_a + h_b}{2h_c} \; ; \quad z_c = 0 \; ; \quad z_k = \pm \tfrac{h_k + h_c}{2} \; ; \quad h_k = \textstyle\sum_j^{n,m} h_{k_j}$$

n and m are the numbers of sub-layers of the upper a and lower b faces, respectively. $\bullet'$ states for $\partial \bullet / \partial x$.

The sandwich beam displacements [1] are entirely defined by the mean $\bar{u} = (u_a + u_b)/2$ and relative $\tilde{u} = u_a - u_b$ axial displacements of the face sheets mid-planes, the transverse deflection w and its derivative w'. Hence, using Lagrange linear shape functions for the axial mean and relative displacements and Hermite cubic ones for the

transverse deflection, leads to a finite element with four degrees of freedom (dof) at each node. The interpolation of the generalized displacements $\mathbf{d} = \text{col}(\bar{u},\ \tilde{u},\ w)$ may then be written as

$$\mathbf{d} = \mathbf{N}\mathbf{q}_e \qquad [2]$$

where

$$\mathbf{N} = \begin{bmatrix} 1-\xi & 0 & 0 & 0 & \xi & 0 & 0 & 0 \\ 0 & 0 & 0 & 1-\xi & 0 & 0 & 0 & \xi \\ 0 & 1-3\xi^2+2\xi^3 & (\xi-2\xi^2+\xi^3)L_e & 0 & 0 & 3\xi^2-2\xi^3 & (-\xi^2+\xi^3)L_e & 0 \end{bmatrix}$$

is the interpolation matrix with $\xi = x/L_e$ and L_e, the element length. $\mathbf{q}_e$ is the element dof vector given by

$$\mathbf{q}_e = \text{col}(\bar{u}_1, w_1, w_1', \tilde{u}_1, \bar{u}_2, w_2, w_2', \tilde{u}_2) \qquad [3]$$

where col( ) is used to define column vectors. Using [1] and [2], the displacements of the faces $\mathbf{u}_k = \text{col}(u_k, \beta_k, w)$ and the core $\mathbf{u}_c = \text{col}(u_c, \beta_c, w)$ are then discretized as follows

$$\mathbf{u}_k = \mathbf{R}_k\mathbf{d} = \mathbf{H}_k\mathbf{q}_e\ ; \quad \mathbf{u}_c = \mathbf{R}_c\mathbf{d} = \mathbf{H}_c\mathbf{q}_e \qquad [4]$$

where

$$\mathbf{R}_k = \begin{bmatrix} 1 & \pm\frac{1}{2} & 0 \\ 0 & 0 & -\frac{\partial}{\partial x} \\ 0 & 0 & 1 \end{bmatrix}\ ;\ k = a(+), b(-)\ ; \quad \mathbf{R}_c = \begin{bmatrix} 1 & 0 & d\frac{\partial}{\partial x} \\ 0 & \frac{1}{h_c} & \lambda\frac{\partial}{\partial x} \\ 0 & 0 & 1 \end{bmatrix}$$

$\mathbf{H}_k = \mathbf{R}_k\mathbf{N}$, $\mathbf{H}_c = \mathbf{R}_c\mathbf{N}$ are the faces and core displacement operators, respectively.

From the usual strain-displacement relations and using [1], axial and shear strains of the faces and the core may be written as

$$\varepsilon_{1i} = \varepsilon_i^m + (z - z_i)\varepsilon_i^b\ ;\ \varepsilon_{5c} = \varepsilon_c^s\ ; \quad i = a, b, c \qquad [5]$$

where membrane ε_i^m, bending ε_i^b and shear ε_c^s strains are

$$\varepsilon_k^m = \bar{u}' \pm \frac{\tilde{u}'}{2}\ ;\ \varepsilon_k^b = -w''\ ;\ \varepsilon_c^m = \bar{u}' + dw''\ ;\ \varepsilon_c^b = \frac{\tilde{u}'}{h_c} + \lambda w''\ ;\ \varepsilon_c^s = \frac{\tilde{u}}{h_c} + (\lambda+1)w'$$

Using [2] and [5], the strains of the faces $\boldsymbol{\varepsilon}_k = \text{col}(\varepsilon_k^m, \varepsilon_k^b)$ and the core $\boldsymbol{\varepsilon}_c = \text{col}(\varepsilon_c^m, \varepsilon_c^b, \varepsilon_c^s)$ are then discretized as follows

$$\boldsymbol{\varepsilon}_k = \mathbf{L}_k\mathbf{d} = \mathbf{B}_k\mathbf{q}_e\ ; \quad \boldsymbol{\varepsilon}_c = \mathbf{L}_c\mathbf{d} = \mathbf{B}_c\mathbf{q}_e \qquad [6]$$

where $\mathbf{B}_k = \mathbf{L}_k\mathbf{N}$, $\mathbf{B}_c = \mathbf{L}_c\mathbf{N}$ are the strain operators for the faces and the core, respectively, and

$$\mathbf{L}_k = \begin{bmatrix} \dfrac{\partial}{\partial x} & \pm\dfrac{1}{2}\dfrac{\partial}{\partial x} & 0 \\ 0 & 0 & -\dfrac{\partial^2}{\partial x^2} \end{bmatrix} \; ; k = a(+), b(-) \; ; \quad \mathbf{L}_c = \begin{bmatrix} \dfrac{\partial}{\partial x} & 0 & d\dfrac{\partial^2}{\partial x^2} \\ 0 & \dfrac{1}{h_c}\dfrac{\partial}{\partial x} & \lambda\dfrac{\partial^2}{\partial x^2} \\ 0 & \dfrac{1}{h_c} & (\lambda+1)\dfrac{\partial}{\partial x} \end{bmatrix}$$

2.2. *Reduced constitutive equations*

The piezoelectric materials are assumed linear orthotropic with material symmetry axes parallel to those of the beam. Their elastic, piezoelectric and dielectric constants are denoted by c_{ij}, e_{lj} and ϵ_{ll} $(i,j = 1,...,6; l = 1,2,3)$. All layers will be considered piezoelectric, where piezoelectric constants are set to vanish for elastic and viscoelastic layers. The three-dimensional linear constitutive equations of an orthotropic piezoelectric layer can be reduced to

$$\sigma_1 = c_{11}^*\varepsilon_1 - e_{31}^* E_3 \; ; \; \sigma_{5c} = c_{55}^c\varepsilon_{5c} \; ; \; D_3 = e_{31}^*\varepsilon_1 + \epsilon_{33}^* E_3 \qquad [7]$$

where

$$c_{11}^* = c_{11} - \frac{c_{13}^2}{c_{33}} \; ; \; e_{31}^* = e_{31} - \frac{c_{13}}{c_{33}}e_{33} \; ; \; \epsilon_{33}^* = \epsilon_{33} + \frac{e_{33}^2}{c_{33}}$$

This reduction is detailed in [BEN 97]. σ_1 and σ_5 are axial and shear components of stress, and D_3 and E_3 are transverse electrical displacement and field. From [7], one may notice that the piezoelectric effect couples the axial strain and transverse electrical field. This is the conventional piezoelectric extension actuation mechanism. Its comparison with the shear actuation mechanism can be found in [BEN 00].

The electrical field E_{3k_j} is assumed constant and induced by a difference of potential V_{k_j} applied on the k_j-th piezoelectric sub-layer, such that

$$E_{3k_j} = -V_{k_j}/h_{k_j} \qquad [8]$$

2.3. *Element stiffness matrix*

The virtual work of electromechanical internal forces of the k_j-th face piezoelectric laminae is

$$\delta H_{k_j} = \int_{\Omega_{k_j}} \left(\delta\varepsilon_{1k}\sigma_{1k_j} - \delta E_{3k_j}D_{3k_j}\right) d\Omega_{k_j} \; ; \quad k_j = a_1,\ldots,a_n,b_1,\ldots,b_m \qquad [9]$$

Introducing [7] and [8], the virtual work δH_{k_j} can be written, for a given V_{k_j}, as

$$\delta H_{k_j} = \delta H_{k_j m} - \delta H_{k_j em} \qquad [10]$$

where

$$\delta H_{k_j m} = \int_{\Omega_{k_j}} \delta\varepsilon_{1k} c_{11}^{*k_j} \varepsilon_{1k}\, d\Omega_{k_j} \; ; \; \delta H_{k_j em} = -\int_{\Omega_{k_j}} \delta\varepsilon_{1k} e_{31}^{*k_j} \frac{V_{k_j}}{h_{k_j}}\, d\Omega_{k_j}$$

The term $-e_{31}^{*k_j} V_{k_j}/h_{k_j}$ may be considered as a piezoelectric stress induced by the applied electrical field on the k_j-th piezoelectric laminae. Consequently, the second term of [10] will be considered as the virtual variation of the work of electrical loads and detailed in the next section.

Integrating through-thickness the mechanical internal virtual work $\delta H_{k_j m}$, and using [5] and [6], the discretization of $\delta H_{k_j m}$ leads to the following elementary virtual work

$$\delta H_{k_j m}^e = \delta \mathbf{q}_e^T \mathbf{K}_{k_j}^e \mathbf{q}_e \qquad [11]$$

with $\mathbf{K}_{k_j}^e$ being the elementary stiffness matrix of the k_j-th face laminae,

$$\mathbf{K}_{k_j}^e = \int_0^{L_e} \mathbf{B}_k^T \mathbf{D}_{k_j} \mathbf{B}_k\, dx \; ; \quad \mathbf{D}_{k_j} = c_{11}^{*k_j} \begin{bmatrix} A_{k_j} & \bar{I}_{k_j} \\ \bar{I}_{k_j} & I_{k_j} \end{bmatrix} \qquad [12]$$

A_{k_j}, $\bar{I}_{k_j}$ and I_{k_j} are the cross section area and first and second moments of inertia of the k_j-th sub-layer face, respectively. The elementary stiffness matrix of the face sheets is then obtained by adding each laminae stiffness contribution

$$\mathbf{K}_f^e = \sum_{k=a}^{b} \sum_{j=1}^{n,m} \mathbf{K}_{k_j}^e \qquad [13]$$

The stiffness contribution of the viscoelastic core can be found from its mechanical internal virtual work, which is composed of axial and shear strains contributions,

$$\delta H_{cm} = \int_{\Omega_c} (\delta\varepsilon_{1c}\sigma_{1c} + \delta\varepsilon_{5c}\sigma_{5c})\, d\Omega_c \qquad [14]$$

Integrating through-thickness this expression and using [5], [6] and [7], its virtual variation δH_{cm} may be discretized, leading to its element contribution

$$\delta H_{cm}^e = \delta \mathbf{q}_e^T \mathbf{K}_c^e \mathbf{q}_e \qquad [15]$$

where the elementary stiffness matrix of the core is

$$\mathbf{K}_c^e = \int_0^{L_e} \mathbf{B}_c^T \mathbf{D}_c \mathbf{B}_c \, dx \; ; \quad \mathbf{D}_c = \begin{bmatrix} c_{11}^{*c} A_c & 0 & 0 \\ 0 & c_{11}^{*c} I_c & 0 \\ 0 & 0 & k_c c_{55}^c A_c \end{bmatrix} \qquad [16]$$

k_c is the shear correction factor.

The elementary stiffness matrix of the sandwich beam finite element is obtained by summation of the face sheets and core contributions

$$\mathbf{K}^e = \mathbf{K}_f^e + \mathbf{K}_c^e \qquad [17]$$

It is worthwhile to notice that each face sub-layer stiffness matrix [12] is composed of membrane and bending strains and a membrane-bending coupling term, due to the distance between the mid-plan of each sub-layer and its corresponding layer.

2.4. *Element piezoelectric loads vector*

Using [5]–[8], the element contribution to the virtual variation of the generalized piezoelectric loads work $H_{k_j em}$ [10], induced by the applied electrical field, may be discretized, for the k_j-th face piezoelectric laminae, as

$$\delta H_{k_j em}^e = \delta \mathbf{q}_e^T \mathbf{F}_{k_j e}^e \qquad [18]$$

where the elementary equivalent piezoelectric load vector $\mathbf{F}_{k_j e}^e$ is

$$\mathbf{F}_{k_j e}^e = -\int_0^{L_e} \mathbf{B}_k^T \mathbf{D}_{k_j e} \frac{V_{k_j}}{h_{k_j}} \, dx \; ; \quad \mathbf{D}_{k_j e} = e_{31}^{*k_j} \begin{bmatrix} A_{k_j} \\ \bar{I}_{k_j} \end{bmatrix} \qquad [19]$$

The applied generalized piezoelectric loads vector of the element is the sum of those of each face sub-layer

$$\mathbf{F}_e^e = \sum_{k=a}^{b} \sum_{j=1}^{n,m} \mathbf{F}_{k_j e}^e \qquad [20]$$

2.5. *Element mass matrix*

The elementary mass matrix of the sandwich beam may be obtained from the virtual variation of the works of inertial forces, which are, for the k_j-th face sub-layer

and the core,

$$\delta T_{k_j} = -\int_{\Omega_{k_j}} \rho_{k_j} \left(\delta \breve{u}_k \ddot{\breve{u}}_k + \delta w \ddot{w}\right) d\Omega_{k_j} \; ; \; \delta T_c = -\int_{\Omega_c} \rho_c \left(\delta \breve{u}_c \ddot{\breve{u}}_c + \delta w \ddot{w}\right) d\Omega_c \quad [21]$$

where ρ states for the volumic mass density and $\dot{\bullet}$ states for $\partial \bullet / \partial t$.

Integrating through-thickness expression [21] and using [1] and [4], elementary contributions of δT_{k_j} and δT_c are discretized as

$$\delta T^e_{k_j} = -\delta \mathbf{q}^T_e \mathbf{M}^e_{k_j} \ddot{\mathbf{q}}_e \; ; \; \delta T^e_c = -\delta \mathbf{q}^T_e \mathbf{M}^e_c \ddot{\mathbf{q}}_e \quad [22]$$

with $\mathbf{M}^e_{k_j}$ and $\mathbf{M}^e_c$ being the elementary mass matrices of the k_j-th face laminae and the core, respectively,

$$\mathbf{M}^e_{k_j} = \int_0^{L_e} \mathbf{H}^T_k \mathbf{I}_{k_j} \mathbf{H}_k \, dx \; ; \; \mathbf{M}^e_c = \int_0^{L_e} \mathbf{H}^T_c \mathbf{I}_c \mathbf{H}_c \, dx \quad [23]$$

where

$$\mathbf{I}_{k_j} = \rho_{k_j} \begin{bmatrix} A_{k_j} & \bar{I}_{k_j} & 0 \\ \bar{I}_{k_j} & I_{k_j} & 0 \\ 0 & 0 & A_{k_j} \end{bmatrix} \; ; \; \mathbf{I}_c = \rho_c \begin{bmatrix} A_c & 0 & 0 \\ 0 & I_c & 0 \\ 0 & 0 & A_c \end{bmatrix}$$

The elementary mass matrix of the face sheets is then obtained by adding each face sub-layer contribution

$$\mathbf{M}^e_f = \sum_{k=a}^{b} \sum_{j=1}^{n,m} \mathbf{M}^e_{k_j} \quad [24]$$

Finally, the sandwich beam finite element mass matrix is obtained by summation of the face sheets and core contributions

$$\mathbf{M}^e = \mathbf{M}^e_f + \mathbf{M}^e_c \quad [25]$$

As for the stiffness matrix, one may notice that each face sub-layer mass matrix [23] is composed of axial and transversal translations and rotation in the xz-plan inertial contributions and an axial translation-rotation inertia coupling term, due also to the distance between the mid-plan of each sub-layer and its corresponding layer.

2.6. *Discretized equations of motion*

Assembling discretized expressions of elementary virtual works [11], [15], [18], [22], and their corresponding matrices [17], [25] and vectors [20], for all elements and

using d'Alembert's principle, the following discretized equations of motion may be written

$$\mathbf{M}\ddot{\mathbf{q}} + \mathbf{D}\dot{\mathbf{q}} + \mathbf{K}\mathbf{q} = \mathbf{F}_m + \mathbf{F}_e \qquad [26]$$

where a viscous damping matrix $\mathbf{D}$ and a mechanical nodal load vector $\mathbf{F}_m$ have been considered a posteriori. $\mathbf{M}$, $\mathbf{K}$, $\mathbf{F}_e$ are the global mass and stiffness matrices, and piezoelectric loads vector, of the whole sandwich beam.

3. Viscoelastic damping models

Since the core is made of a viscoelastic material, one must take into account the frequency-and-temperature-dependence of its stiffness and damping properties. Supposing a constant Poisson's ratio, the equations of motion [26] are re-written as

$$\mathbf{M}\ddot{\mathbf{q}} + \mathbf{D}\dot{\mathbf{q}} + [\mathbf{K}_f + G^*(\omega,\theta)\bar{\mathbf{K}}_c]\mathbf{q} = \mathbf{F}_m + \mathbf{F}_e \qquad [27]$$

where $G^*(\omega,\theta)$ is the frequency-and-temperature-dependent complex shear modulus of the core and $\bar{\mathbf{K}}_c$ is the modulus factored-out core stiffness matrix. In the following subsections, three methods to account for the frequency-dependence of the last equation, considering a fixed temperature, are presented. Then, for analysis of the temperature variation effects, viscoelastic material is modeled using such methods for several operating temperatures.

3.1. *Golla-Hughes-McTavish model*

The GHM model represents the material shear modulus as a series of functions, in the Laplace domain, such that [MCT 93]

$$sG(s) = G_0\left(1 + \sum_i \hat{\alpha}_i \frac{s^2 + 2\hat{\zeta}_i\hat{\omega}_i s}{s^2 + 2\hat{\zeta}_i\hat{\omega}_i s + \hat{\omega}_i^2}\right) \qquad [28]$$

where G_0 represents the relaxed modulus, or static modulus. Notice that, from [28], the unrelaxed modulus may be written as $G_\infty = G_0(1 + \sum_i \hat{\alpha}_i)$. Each function in the series is dependent on three material constants, namely $\hat{\alpha}_i$, $\hat{\omega}_i$ and $\hat{\zeta}_i$, evaluated from curve-fitting of the viscoelastic material master curves. Substituting [28] in the Laplace-transformed equations of motion [27] leads to

$$\left[s^2\mathbf{M} + s\mathbf{D} + \mathbf{K}_f + \mathbf{K}_c^0\left(1 + \sum_i \hat{\alpha}_i \frac{s^2 + 2\hat{\zeta}_i\hat{\omega}_i s}{s^2 + 2\hat{\zeta}_i\hat{\omega}_i s + \hat{\omega}_i^2}\right)\right]\tilde{\mathbf{q}}(s) = \tilde{\mathbf{F}}_m(s) + \tilde{\mathbf{F}}_e(s) \qquad [29]$$

with $\mathbf{K}_c^0 = G_0 \bar{\mathbf{K}}_c$ being the core static stiffness. Introducing a series of n dissipative variables $\mathbf{z}_i$ $(i = 1, \ldots, n)$ such that,

$$\tilde{\mathbf{z}}_i(s) = \frac{\hat{\omega}_i^2}{s^2 + 2\hat{\zeta}_i \hat{\omega}_i s + \hat{\omega}_i^2} \tilde{\mathbf{q}}(s) \qquad [30]$$

one may write the following augmented system

$$\left(s^2 \mathbf{M} + s\mathbf{D} + \mathbf{K}_f + \mathbf{K}_c^\infty\right) \tilde{\mathbf{q}}(s) - \mathbf{K}_c^0 \sum_i \hat{\alpha}_i \tilde{\mathbf{z}}_i(s) = \tilde{\mathbf{F}}_m(s) + \tilde{\mathbf{F}}_e(s) \qquad [31a]$$

$$\left(s^2 \frac{1}{\hat{\omega}_i^2} + s \frac{2\hat{\zeta}_i}{\hat{\omega}_i} + 1\right) \tilde{\mathbf{z}}_i(s) - \tilde{\mathbf{q}}(s) = 0 \qquad [31b]$$

where $\mathbf{K}_c^\infty = \mathbf{K}_c^0 (1 + \sum_i \hat{\alpha}_i)$ is the unrelaxed, or high-frequency, core stiffness. Multiplying equations [31b] by $\hat{\alpha}_i \mathbf{K}_c^0$ and retransforming [31] to time-domain, it becomes

$$\bar{\mathbf{M}} \ddot{\bar{\mathbf{q}}} + \bar{\mathbf{D}} \dot{\bar{\mathbf{q}}} + \bar{\mathbf{K}} \bar{\mathbf{q}} = \bar{\mathbf{F}} \qquad [32]$$

with

$$\bar{\mathbf{M}} = \begin{bmatrix} \mathbf{M} & \mathbf{0} \\ \mathbf{0} & \mathbf{M}_{zz} \end{bmatrix} ; \bar{\mathbf{D}} = \begin{bmatrix} \mathbf{D} & \mathbf{0} \\ \mathbf{0} & \mathbf{D}_{zz} \end{bmatrix} ; \bar{\mathbf{K}} = \begin{bmatrix} \mathbf{K}_f + \mathbf{K}_c^\infty & \mathbf{K}_{qz} \\ \mathbf{K}_{qz}^T & \mathbf{K}_{zz} \end{bmatrix}$$

$$\bar{\mathbf{q}} = \mathrm{col}(\mathbf{q}, \mathbf{z}_1, \ldots, \mathbf{z}_n) ; \bar{\mathbf{F}} = \mathrm{col}(\mathbf{F}_m + \mathbf{F}_e, \mathbf{0}, \ldots, \mathbf{0})$$

and

$$\mathbf{M}_{zz} = \begin{bmatrix} \frac{\hat{\alpha}_1}{\hat{\omega}_1^2} \mathbf{K}_c^0 & & \mathbf{0} \\ & \ddots & \\ \mathbf{0} & & \frac{\hat{\alpha}_n}{\hat{\omega}_n^2} \mathbf{K}_c^0 \end{bmatrix} ; \mathbf{D}_{zz} = \begin{bmatrix} \frac{2\hat{\alpha}_1 \hat{\zeta}_1}{\hat{\omega}_1} \mathbf{K}_c^0 & & \mathbf{0} \\ & \ddots & \\ \mathbf{0} & & \frac{2\hat{\alpha}_n \hat{\zeta}_n}{\hat{\omega}_n} \mathbf{K}_c^0 \end{bmatrix}$$

$$\mathbf{K}_{zz} = \begin{bmatrix} \hat{\alpha}_1 \mathbf{K}_c^0 & & \mathbf{0} \\ & \ddots & \\ \mathbf{0} & & \hat{\alpha}_n \mathbf{K}_c^0 \end{bmatrix} ; \mathbf{K}_{qz} = \begin{bmatrix} -\hat{\alpha}_1 \mathbf{K}_c^0 & \cdots & -\hat{\alpha}_n \mathbf{K}_c^0 \end{bmatrix}$$

Although this form is quite simple, its mass matrix is non-singular only for totally covered beams, for which $\mathbf{K}_c^0$ is also non-singular. Therefore, for the general case, one may either substitute the singular $\mathbf{K}_c^0$ matrix by the identity matrix in the second block line of the matrices of [32], leading to a non-singular mass matrix but also to an asymmetric stiffness matrix ($\mathbf{K}_{zq} \neq \mathbf{K}_{qz}^T$), or, otherwise, use a modal reduction of the matrix $\mathbf{K}_c^0$, such that $\Phi_i^d = \mathbf{T}^T \mathbf{z}_i$ and $\Lambda = \mathbf{T}^T \bar{\mathbf{K}}_c \mathbf{T}$. Where Λ is the non vanishing $\bar{\mathbf{K}}_c$ eigenvalues matrix and $\mathbf{T}$ its corresponding eigenvectors matrix. In this case, the mass matrix is non-singular, the stiffness matrix is symmetric and, also, the matrices corresponding to dissipative variables are diagonalized and eventually reduced. Hence, the

matrices $\mathbf{M}_{zz}$, $\mathbf{D}_{zz}$, $\mathbf{K}_{zz}$ and $\mathbf{K}_{qz}$ of [32] are rewritten as

$$\mathbf{M}_{zz} = \begin{bmatrix} \frac{\hat{\alpha}_1}{\hat{\omega}_1^2} G_0\Lambda & & \mathbf{0} \\ & \ddots & \\ \mathbf{0} & & \frac{\hat{\alpha}_n}{\hat{\omega}_n^2} G_0\Lambda \end{bmatrix} ; \mathbf{D}_{zz} = \begin{bmatrix} \frac{2\hat{\alpha}_1\hat{\zeta}_1}{\hat{\omega}_1} G_0\Lambda & & \mathbf{0} \\ & \ddots & \\ \mathbf{0} & & \frac{2\hat{\alpha}_n\hat{\zeta}_n}{\hat{\omega}_n} G_0\Lambda \end{bmatrix}$$

$$\mathbf{K}_{zz} = \begin{bmatrix} G_0\Lambda & & \mathbf{0} \\ & \ddots & \\ \mathbf{0} & & G_0\Lambda \end{bmatrix} ; \mathbf{K}_{qz} = \begin{bmatrix} -\hat{\alpha}_1\mathbf{K}_c^0\mathbf{T} & \cdots & -\hat{\alpha}_n\mathbf{K}_c^0\mathbf{T} \end{bmatrix}$$

This method allows both a good representation of the frequency-dependence of viscoelastic materials and time-domain analyses of the augmented system, since all of its matrices are constants.

3.2. *Anelastic Displacement Fields model*

The ADF model, proposed in [LES 95, LES 96b], represents the complex material modulus as a series of functions in the frequency-domain, such that

$$G^*(\omega) = G_0\left(1 + \sum_i \Delta_i \frac{\omega^2 + j\omega\,\Omega_i}{\omega^2 + \Omega_i^2}\right) \qquad [33]$$

where, here, the unrelaxed modulus is $G_\infty = G_0(1 + \sum_i \Delta_i)$. Ω_i and Δ_i are material parameters evaluated from curve-fitting of material master curves.

This method is based on the separation of viscoelastic material strains in elastic and anelastic parts. The first one is instantaneously proportional to the stress and represents the energy storage, whereas the other represents material relaxation and, thus, dissipation. This separation may be obtained by introducing a series of dissipative variables $\mathbf{q}_i^a$ $(i = 1, \ldots, n)$, such that

$$\mathbf{q}^e = \mathbf{q} - \sum_i \mathbf{q}_i^a \qquad [34]$$

The variables $\mathbf{q}^e$ replace then $\mathbf{q}$ in the core strain internal work expression, leading to

$$\mathbf{M}\ddot{\mathbf{q}} + \mathbf{D}\dot{\mathbf{q}} + (\mathbf{K}_f + \mathbf{K}_c^\infty)\mathbf{q} - \mathbf{K}_c^\infty \sum_i \mathbf{q}_i^a = \mathbf{F}_m + \mathbf{F}_e \qquad [35]$$

where, here, the unrelaxed stiffness of the core is $\mathbf{K}_c^\infty = (1 + \sum_i \Delta_i)\mathbf{K}_c^0$. In addition to the last expression, one should write a system of equations describing the relaxation

process

$$\frac{C_i}{\Omega_i}\mathbf{K}_c^{\infty}\dot{\mathbf{q}}_i^a - \mathbf{K}_c^{\infty}\mathbf{q} + C_i\mathbf{K}_c^{\infty}\mathbf{q}_i^a = 0 \qquad [36]$$

where the material parameters C_i are related to Δ_i such that $C_i = (1+\sum_i \Delta_i)/\Delta_i$. Combining equations [35] and [36] leads to

$$\bar{\mathbf{M}}\ddot{\bar{\mathbf{q}}} + \bar{\mathbf{D}}\dot{\bar{\mathbf{q}}} + \bar{\mathbf{K}}\bar{\mathbf{q}} = \bar{\mathbf{F}} \qquad [37]$$

where

$$\bar{\mathbf{M}} = \begin{bmatrix} \mathbf{M} & \mathbf{0} \\ \mathbf{0} & \mathbf{0} \end{bmatrix} ; \bar{\mathbf{D}} = \begin{bmatrix} \mathbf{D} & \mathbf{0} \\ \mathbf{0} & \mathbf{D}_{aa} \end{bmatrix} ; \bar{\mathbf{K}} = \begin{bmatrix} \mathbf{K}_f + \mathbf{K}_c^{\infty} & \mathbf{K}_{ea} \\ \mathbf{K}_{ea}^T & \mathbf{K}_{aa} \end{bmatrix}$$

$$\bar{\mathbf{q}} = \mathrm{col}(\mathbf{q}, \mathbf{q}_1^a, \ldots, \mathbf{q}_n^a) ; \bar{\mathbf{F}} = \mathrm{col}(\mathbf{F}_m + \mathbf{F}_e, \mathbf{0}, \ldots, \mathbf{0})$$

with

$$\mathbf{D}_{aa} = \begin{bmatrix} \frac{C_1}{\Omega_1}\mathbf{K}_c^{\infty} & & \mathbf{0} \\ & \ddots & \\ \mathbf{0} & & \frac{C_n}{\Omega_n}\mathbf{K}_c^{\infty} \end{bmatrix} ; \mathbf{K}_{aa} = \begin{bmatrix} C_1\mathbf{K}_c^{\infty} & & \mathbf{0} \\ & \ddots & \\ \mathbf{0} & & C_n\mathbf{K}_c^{\infty} \end{bmatrix}$$

$$\mathbf{K}_{ea} = \begin{bmatrix} -\mathbf{K}_c^{\infty} & \cdots & -\mathbf{K}_c^{\infty} \end{bmatrix}$$

As for GHM model, one may propose a modal reduction of matrix $\mathbf{K}_c^{\infty}$ to diagonalize matrices and reduce augmented system dimension. Hence, let $\Phi_i^d = \mathbf{T}^T\mathbf{q}_i^a$ and $\Lambda = \mathbf{T}^T\bar{\mathbf{K}}_c\mathbf{T}$ so that matrices $\mathbf{D}_{aa}$, $\mathbf{K}_{aa}$ and $\mathbf{K}_{ea}$ could be rewritten as

$$\mathbf{D}_{aa} = \begin{bmatrix} \frac{C_1}{\Omega_1}G_{\infty}\Lambda & & \mathbf{0} \\ & \ddots & \\ \mathbf{0} & & \frac{C_n}{\Omega_n}G_{\infty}\Lambda \end{bmatrix} ; \mathbf{K}_{aa} = \begin{bmatrix} C_1G_{\infty}\Lambda & & \mathbf{0} \\ & \ddots & \\ \mathbf{0} & & C_nG_{\infty}\Lambda \end{bmatrix}$$

$$\mathbf{K}_{ea} = \begin{bmatrix} -\mathbf{K}_c^{\infty}\mathbf{T} & \cdots & -\mathbf{K}_c^{\infty}\mathbf{T} \end{bmatrix}$$

One may notice that, unlike the case of the GHM model, this reduction leads to a singular mass matrix since, in this case, dissipative variables have no inertia. Therefore, instead of solving the second-order system [37], one should construct an odd state-space system with state col($\bar{\mathbf{q}}$, $\dot{\mathbf{q}}$) rather than col($\bar{\mathbf{q}}$, $\dot{\bar{\mathbf{q}}}$) to eliminate this singularity.

3.3. *Iterative modal strain energy model*

An alternative to the internal variables approach, is to use an iterative version of the MSE method [JOH 81]. It considers that the modal loss factor is approximated as

the product of the viscoelastic material loss factor by the fraction of the dissipative energy, present in the viscoelastic material, to the total strain energy. Following this definition, the iterative algorithm of Figure 1 is proposed.

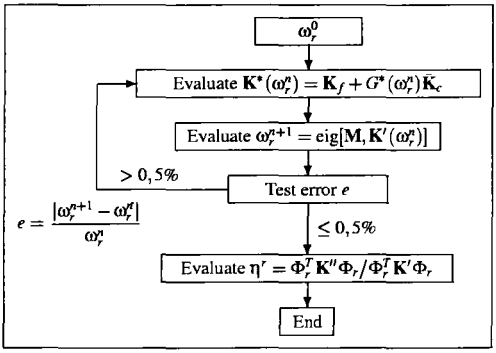

Figure 1. *Iterative modal strain energy algorithm* ($\mathbf{K}' = \Re(\mathbf{K}^*), \mathbf{K}'' = \Im(\mathbf{K}^*)$).

Using such an algorithm, undamped eigenfrequencies and eigenvectors can be correctly evaluated and modal low damping well approximated. The convergence is very fast, however, evaluation must be repeated for each frequency of interest. This technique prevents the evaluation of the state-space system complex modes as in [FRI 98], reducing greatly the computation cost.

To extend this method to the control synthesis, where several modes are excited simultaneously by the controller, let us consider the following eigenfrequency, modal loss factor and eigenvector matrices for the m frequencies of interest ($r = 1, \ldots, m$),

$$\Omega_e = \begin{bmatrix} \omega_1 & & \\ & \ddots & \\ & & \omega_m \end{bmatrix} ; \quad \eta = \begin{bmatrix} \eta^1 & & \\ & \ddots & \\ & & \eta^m \end{bmatrix} ; \quad \mathbf{T}_e = \begin{bmatrix} \Phi_1 & \cdots & \Phi_m \end{bmatrix} \qquad [38]$$

The viscoelastic damping matrix may be approximated by $\eta\Omega_e$. Consequently, the system [27] may be rewritten as

$$\ddot{\hat{\mathbf{q}}} + (2\zeta\mathbf{I} + \eta)\Omega_e\dot{\hat{\mathbf{q}}} + \Omega_e^2\hat{\mathbf{q}} = \mathbf{T}_e^T(\mathbf{F}_e + \mathbf{F}_m) \qquad [39]$$

where the viscous damping matrix $\mathbf{D}$ is assumed to be such that $\mathbf{T}_e^T\mathbf{D}\mathbf{T}_e = 2\zeta\Omega_e$, ζ being the viscous damping factor. Evidently, $\mathbf{T}_e$ may not diagonalize $\mathbf{K}' = \Re(\mathbf{K}^*)$, since each column of $\mathbf{T}_e$ is valid only for a single frequency. Nevertheless, this system constitutes a reasonable approximation of [27] for lightly damped structures.

4. Reduced state-space equations

To apply the frequency-dependent finite element models, presented in the previous sections, to an optimal control synthesis, one may write the second-order equations [32],[37,[39] as a first-order state-space equation

$$\begin{aligned} \dot{\mathbf{x}} &= \mathbf{A}\mathbf{x} + \mathbf{B}\mathbf{u} + \mathbf{p} \\ \mathbf{y} &= \mathbf{C}\mathbf{x} \end{aligned} \qquad [40]$$

Construction of state-space system and corresponding matrices, for each model, are detailed in [TRI 99] and the state vectors $\mathbf{x}$, for GHM, ADF and MSE models, are, respectively,

$$\mathbf{x} = \begin{bmatrix} \bar{\mathbf{q}} \\ \dot{\bar{\mathbf{q}}} \end{bmatrix}, \ \mathbf{x} = \begin{bmatrix} \bar{\mathbf{q}} \\ \dot{\mathbf{q}} \end{bmatrix}, \ \mathbf{x} = \begin{bmatrix} \hat{\mathbf{q}} \\ \dot{\hat{\mathbf{q}}} \end{bmatrix} \qquad [41]$$

However, even with a possible reduction of extra dissipative dofs in ADF and GHM models, the state-space system [40] is too large for use in the control synthesis. Thus, a modal reduction technique is proposed to reduce the system dimension and also to allow a better comparison between the three viscoelastic damping models presented previously. The eigensolution of the state-space matrix $\mathbf{A}$ is then evaluated

$$\mathbf{A}\mathbf{T}_r = \Lambda\mathbf{T}_r \ ; \ \mathbf{A}^T\mathbf{T}_l = \Lambda\mathbf{T}_l \qquad [42]$$

where the right $\mathbf{T}_r$ and left $\mathbf{T}_l$ complex eigenvectors are then normalized by $\mathbf{T}_l^T\mathbf{T}_r = \mathbf{I}$.

Let us consider a modal decomposition of the eigenvalues matrix Λ in the form

$$\Lambda = \begin{bmatrix} \Lambda_e & \mathbf{0} \\ \mathbf{0} & \Lambda_d \end{bmatrix} \qquad [43]$$

where Λ_e and Λ_d are the eigenvalues sub-matrices corresponding to the elastic and dissipative dofs, respectively. Similarly, the right and left eigenvectors $\mathbf{T}_r$ and $\mathbf{T}_l$ are composed of elastic and dissipative eigenmodes associated to Λ_e and Λ_d,

$$\mathbf{T}_r = [\mathbf{T}_{re} \ \mathbf{T}_{rd}] \ ; \ \mathbf{T}_l = [\mathbf{T}_{le} \ \mathbf{T}_{ld}] \qquad [44]$$

Generally, the eigenmodes associated to dissipative dofs (relaxation modes) are overdamped, according to [MCT 93]. Consequently, it can be assumed that their contribution to the system response is negligible. Also, considering just a reduced frequency range, one may truncate the modal base neglecting the dynamic contribution of the eigenmodes which eigenvalues lies out of the frequency range. Consequently, the system [40] reduces to

$$\begin{aligned} \dot{\hat{\mathbf{x}}} &= \hat{\mathbf{A}}\hat{\mathbf{x}} + \hat{\mathbf{B}}\mathbf{u} + \hat{\mathbf{p}} \\ \mathbf{y} &= \hat{\mathbf{C}}\hat{\mathbf{x}} \end{aligned} \qquad [45]$$

where $\hat{\mathbf{x}} = \mathbf{T}_{ret}\mathbf{x}$ and $\hat{\mathbf{A}} = \mathbf{T}_{let}^T\mathbf{A}\mathbf{T}_{ret}$; $\hat{\mathbf{B}} = \mathbf{T}_{let}^T\mathbf{B}$; $\hat{\mathbf{p}} = \mathbf{T}_{let}^T\mathbf{p}$; $\hat{\mathbf{C}} = \mathbf{C}\mathbf{T}_{ret}$. $\mathbf{T}_{ret}$ and $\mathbf{T}_{let}$ are the matrices corresponding to the truncated bases of retained eigenmodes.

This modal reduction technique is very simple to implement since the choice of eigenmodes to be retained is based only on the frequency range considered. Nevertheless, for highly damped systems, where elastic modes may also be overdamped, the eigenfrequencies analysis must be associated with an eigenmodes one. Notice that for the iterative MSE method, the reduction may be achieved directly from the iterative algorithm by just evaluating the frequencies inside the frequency range.

5. Constrained optimal control strategy

The Linear Quadratic Regulator (LQR) optimal control algorithm is considered. It consists in the minimization of a cost function J

$$J = \frac{1}{2}\int_0^\infty (\hat{\mathbf{x}}^T\mathbf{Q}\hat{\mathbf{x}} + \mathbf{u}^T\mathbf{R}\mathbf{u})\, dt \qquad [46]$$

subjected to the linear constraints [45]. This results in a linear full-state feedback control law $\mathbf{u} = -\mathbf{K}_g\hat{\mathbf{x}}$, where $\mathbf{K}_g = \mathbf{R}^{-1}\hat{\mathbf{B}}^T\mathbf{P}$ is a constant control gain matrix, written in terms of the matrix $\mathbf{P}$, solution of the algebraic Riccati equation

$$\hat{\mathbf{A}}^T\mathbf{P} + \mathbf{P}\hat{\mathbf{A}} - \mathbf{P}\hat{\mathbf{B}}\mathbf{R}^{-1}\hat{\mathbf{B}}^T\mathbf{P} + \mathbf{Q} = \mathbf{0} \qquad [47]$$

Moreover, for an asymptotically stable controlled system, the minimized cost function may be written as

$$J_{min} = \frac{1}{2}\hat{\mathbf{x}}^T(0)\mathbf{P}\hat{\mathbf{x}}(0) \qquad [48]$$

This algorithm is very simple to use, since the Riccati equation may be solved, and the cost may be evaluated, preliminary to the application of the control feedback gain $\mathbf{K}_g$ to the system. However, its performance rests on the appropriate choice of the weight matrices $\mathbf{Q}$ and $\mathbf{R}$. Furthermore, it does not guarantee that the control input $\mathbf{u}$ is feasible, e.g., electrical fields in piezoelectric actuators are constrained to the coercive or depoling electrical field. Hence, an input constraint condition must be imposed to such optimization.

A technique shown to be simple and effective [TRI 00] is based on an iterative LQR, such that the optimal control input is solved for typical operation conditions and its maximum value is used to modify weight matrices until an optimal control gain satisfies both optimal closed-loop performance and input constraint. The algorithm presented in [TRI 00] is modified here constraining the input weight matrix $\mathbf{R}$ instead of the performance $\mathbf{Q}$ one, although both constraints are equivalent. Figure 2a

shows the typical variation of the first three eigenmodes damping factors (%) with the input weight factor γ ($\mathbf{R} = \gamma\,\mathbf{I}$), the minimized cost function J_{min} and also the maximum voltage V_{max} required to achieve these damping ratios. As expected, damping performance diminishes for increasing input weight factors. Figure 2a also shows the feasible region inside the dotted line square, that is, the region for which the maximum voltage is lower than the saturation voltage of the actuator (in this case, 250 V). The iterative optimal control algorithm of [TRI 00], shown in Figure 2b, consists in finding the maximum damping inside the dotted feasible region (Figure 2a).

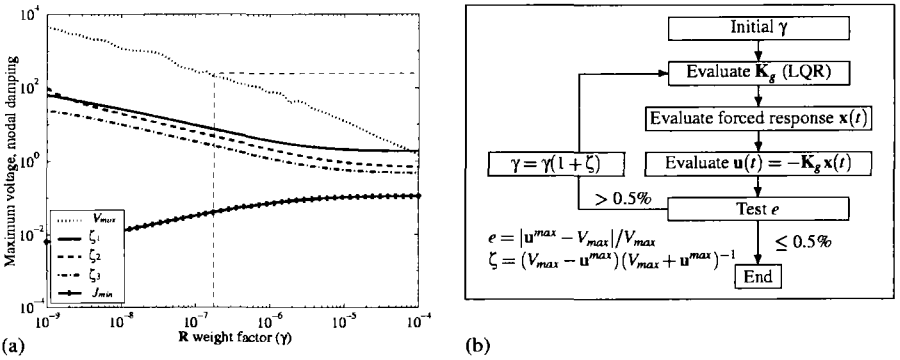

Figure 2. *(a) Maximum voltage and modal damping factors vs. input weight factor γ. (b) Optimal control design under voltage constraint V_{max}.*

It should be noticed that the maximum voltage, shown in Figure 2a, was evaluated from the controlled system response, generated by a given perturbation. Consequently, the control input constraint may not be respected for other load conditions.

In what follows, the performance weight matrix $\mathbf{Q}$ is considered to be diagonal and composed by elements of the output vector $\hat{\mathbf{C}}$, so that $\mathbf{Q} = \text{diag}(|\hat{\mathbf{C}}|)$, to maximize the damping of modes with major contributions to the output, here the tip deflection of a cantilever beam. The γ factor is evaluated so that the maximum electrical field of 500 V/mm on the piezoelectric actuators is not exceeded, for an impulsive transverse perturbation force applied to the beam tip, which magnitude imposes a maximum beam deflection amplitude of 2 mm.

6. Damping performance under temperature variations

The reduced models and control algorithm presented previously are now applied to the analysis of a cantilever beam with a bonded ACLD treatment. The beam is made

of aluminum, with Young's modulus of 70.3 MPa and mass density of 2700 kg m^{-3}, and has a length of 300 mm, a width of 20 mm and a thickness of 2 mm. The hybrid viscoelastic–piezoelectric treatment is made of Soundcoat's Dyad 606 viscoelastic material, 0.25 mm thick and of mass density 1600 kg m^{-3}, and PZT5H piezoelectric ceramic, which Young's modulus is 63.5 MPa, mass density is 7500 kg m^{-3}, piezoelectric constant e_{31}^{*} is -23.2 C m^{-2} and thickness is 0.5 mm. The treatment has a length of 50 mm and is positioned at 10 mm from the clamped end of the beam.

Considering a temperature of 25°C, viscoelastic material properties are used to optimize ADF and GHM parameters in the frequency range 2–3000 Hz. These are used to evaluate the first five bending eigenfrequencies and corresponding damping ratios, shown in Table 1. It can be seen that eigenfrequencies match well for the three models, whereas there is a noticeable difference between MSE damping ratios and ADF and GHM ones. However, this is due to the difficulty of representing the master curves form of this viscoelastic material by ADF and GHM models, although five series of parameters were used.

PCL ADF	23.6 (1.82%)	139.8 (0.66%)	364.3 (0.46%)	676.1 (0.71%)	1105.5 (0.90%)
PCL GHM	23.6 (1.81%)	139.8 (0.67%)	364.3 (0.45%)	676.1 (0.72%)	1105.7 (0.92%)
PCL MSE	23.7 (2.56%)	139.4 (0.99%)	363.6 (0.65%)	673.3 (1.00%)	1099.1 (1.23%)
ACL ADF	23.7 (8.40%)	140.0 (5.41%)	364.3 (3.00%)	676.0 (1.07%)	1105.5 (1.13%)
ACL GHM	23.7 (7.19%)	140.1 (4.59%)	364.2 (2.61%)	676.0 (0.99%)	1105.7 (1.08%)
ACL MSE	23.6 (6.99%)	139.5 (2.78%)	363.6 (0.84%)	673.3 (1.18%)	1099.1 (1.25%)

Table 1. *Open- and closed-loop eigenfrequencies (Hz) and damping factors at 25°C*

Table 1 also shows the closed-loop eigenfrequencies and damping factors (active instead of passive constraining layer). One may see that eigenfrequencies still match but damping ratios for MSE disagree with those of ADF and GHM, since the MSE model is not well adapted for the transient-based control algorithm. However, smaller differences between ADF and GHM damping ratios exist since their eigenmodes, and thus control input vectors, are not exactly the same.

Figure 3a shows the open-loop frequency response function of the cantilever beam tip deflection evaluated using the three viscoelastic models. It can be seen that ADF and GHM results are identical; however, MSE results only match in natural frequencies, that is with almost the same poles but not at all with the same zeros (anti-resonances). This is because neither input nor output matrices are valid over the whole frequency range. In Figure 3b, the equivalent ADF/GHM open-loop frequency response is compared with that of the closed-loop system for these two models. As expected, the controller emphasizes damping of the first mode, although second and third modes are also damped. However, fourth and fifth modes dampings are only slightly increased, since they have little contribution to the output.

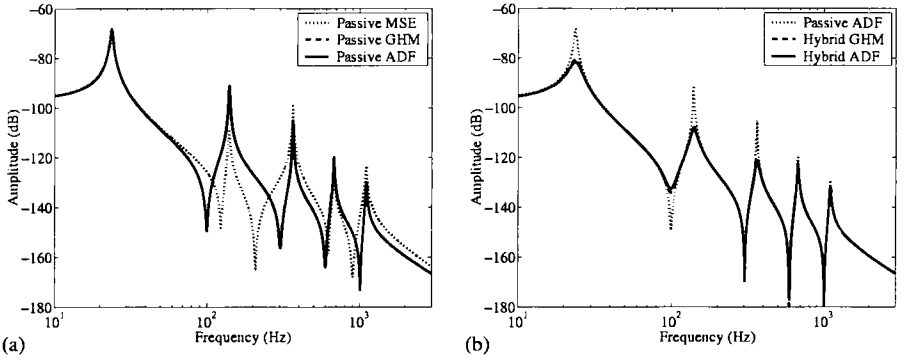

Figure 3. *FRF of the cantilever beam tip deflection: (a) Open-loop response using ADF, GHM and MSE models; (b) Open- vs. closed-loop response*

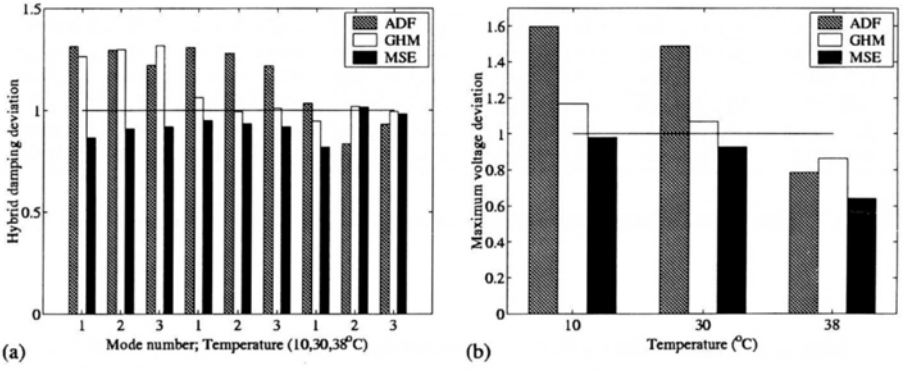

Figure 4. *Deviation of control performance relative to 25°C: (a) Hybrid damping* $(\eta(\theta)/\eta(25))$*; (b) Maximum voltage* $(V_{max}(\theta)/V_{max}(25))$

Thereafter, one might be interested in using the controller designed previously over an operating temperature range. Nevertheless, as viscoelastic material properties change with temperature, damping performance requirements may not be respected. To apply the controller designed at 25°C to the system at different temperatures, the solution of Riccati equation at 25°C $\mathbf{P}_o$ is used to evaluate the control gain $\mathbf{K}_g = \mathbf{R}^{-1}\mathbf{B}^T\mathbf{P}_o$ for the system at different specified temperatures. Figure 4 shows the deviation of hybrid damping and maximum control voltage of the system at temperatures of 10°C, 30°C and 38°C, relative to that at 25°C, when controlled with the controller based on $\mathbf{P}_o$. In Figure 4a, the damping ratios of the first three modes are

drawn for each operating temperature and viscoelastic model. One may notice that for 10°C and 30°C, ADF three first modal dampings augment, however the required maximum voltage also increases (Figure 4b). Similarly, for the other models, an increase in damping is accompanied by an increase in the maximum voltage, thus exceeding the saturation voltage. On the other hand, for 38°C, one may notice an improvement of damping with a diminution of the voltage. However, in this case, one of the modes is further damped (first one for ADF and second one for GHM and MSE), with less voltage, whereas in other modes dampings decrease.

7. Temperature dedicated controller

In consequence of the previous results, one might prefer to design a temperature dedicated controller. Therefore, let us consider four different controllers, one for each operating temperature. In Figure 5, the open- and closed-loop transient responses are drawn for each temperature (10°C, 25°C, 30°C and 38°C). One may notice that, although the open-loop response diminishes faster for higher temperatures, the closed-loop system settles almost equally fast for all temperatures, meaning that the dedicated controller maintains a uniform performance in the temperature range. Since, temperature variations are generally slow, one might envisage evaluating a set of controllers inside an operating temperature range and commuting from one to another as temperature changes. Thus, one may preserve a satisfactory damping performance while respecting control input limitations. Figure 6 shows the control voltage for 10°C and 38°C, where one may notice that both controllers present similar responses. Nevertheless, one may also notice that ADF and GHM do not present the same voltage transient response, although their output responses are very similar (Figures 5a and 5d).

In Figure 7a, the variation of passive damping with temperature shows an increase of all modes damping ratios with increasing temperature, although, from viscoelastic materials nature, damping is expected to start decreasing at a given temperature. It is also worthwhile to analyze the influence of temperature on the hybrid damping gain (relative to passive one), which measures the increase of damping provided by the active control system. Notice that, from Figure 7b, it makes less and less sense using an active controller for higher temperatures since the improvement of damping may not be sufficient to justify the addition of electric cables and filters.

8. Conclusion

A new finite element was presented for sandwich beams with laminate piezoelectric faces and viscoelastic core. Three models were proposed to represent the viscoelastic materials frequency-dependence properties, namely Golla-Hughes-McTavish, Anelastic Displacement Fields and Iterative Modal Strain Energy method. Model re-

ductions were proposed to allow feasible control syntheses. An optimal LQR control algorithm, accounting for input constraints, was presented. Using these open- and closed-loop finite element reduced models, the vibration control of a cantilever beam, through a bonded active constrained layer damping treatment, was analyzed and used to evaluate internal variables approaches. Thereafter, the control performance of hybrid damping treatments was studied under temperature variations. It was found that damping and input requirements may not be respected inside an operating temperature range with a temperature-fixed controller. Consequently, a temperature dedicated controller was analyzed, leading to a satisfactory damping performance, over a 30°C wide temperature range, while respecting input constraints. A similar analysis is being considered to treat other hybrid damping configurations with, for instance, separate active and passive treatments. Geometric and material optimization of active-passive damping treatments is a natural extension of the present work.

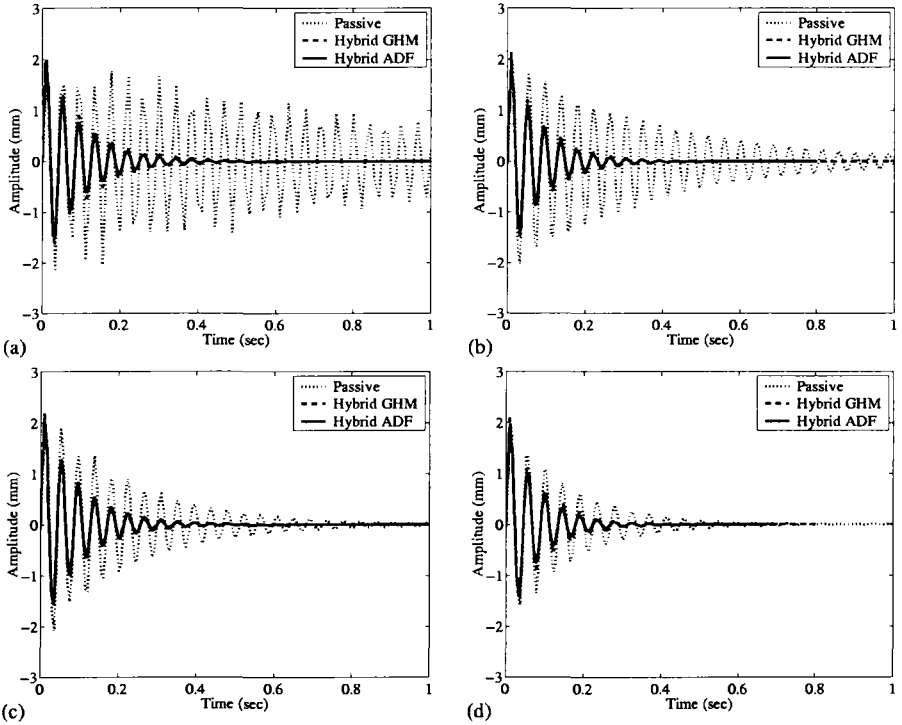

Figure 5. *Open- and closed-loop transient responses for different temperatures: (a) 10°C; (b) 25°C; (c) 30°C; (d) 38°C*

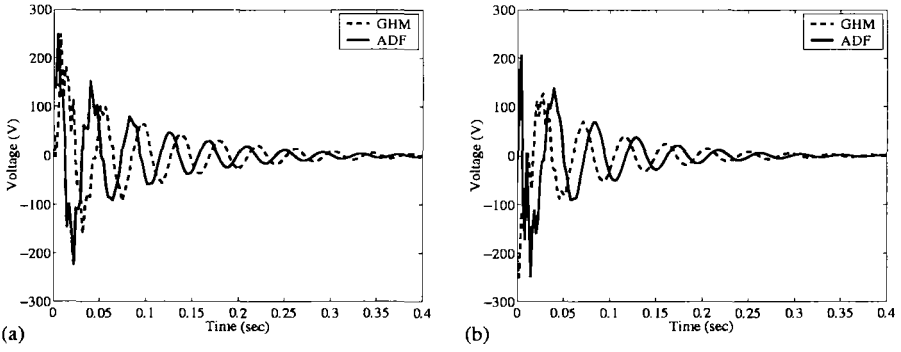

Figure 6. *Control voltage of dedicated controller: (a) at 10°C; (b) at 38°C*

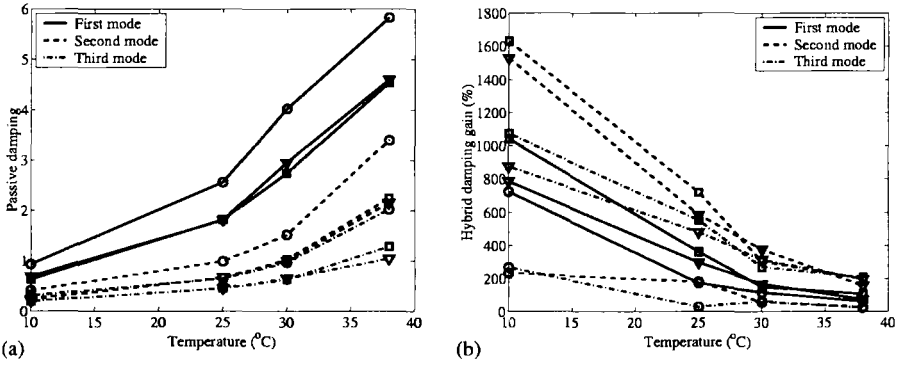

Figure 7. *Variation of damping with temperature: (a) Passive damping; (b) Hybrid damping gain (relative to passive one); ○: MSE; ▽: ADF; □: GHM*

Acknowledgments

Support of the "Délégation Générale pour l'Armement", Advanced Materials Branch, under contract D.G.A./D.S.P./S.T.T.C./MA. 97-2530, is gratefully acknowledged.

9. References

[BEN 97] BENJEDDOU A., TRINDADE M. and OHAYON R., "A unified beam finite element model for extension and shear piezoelectric actuation mechanisms". *J. Intell. Mater. Syst. Struct.*, vol. 8, n° 12, p. 1012–1025, 1997.

[BEN 99a] BENJEDDOU A., "Recent advances in hybrid active-passive vibration control (submitted)". *J. Vib. Control*, 1999.

[BEN 99b] BENJEDDOU A., TRINDADE M. and OHAYON R., "New shear actuated smart structure beam finite element". *AIAA J.*, vol. 37, n° 3, p. 378–383, 1999.

[BEN 00] BENJEDDOU A., TRINDADE M. and OHAYON R., "Piezoelectric actuation mechanisms for intelligent sandwich structures (to appear)". *Smart Mater. Struct.*, vol. 9, 2000.

[FRI 98] FRISWELL M. and INMAN D., "Hybrid damping treatments in thermal environments". In TOMLINSON G. and BULLOUGH W., Eds., *Smart Mater. Struct.*, p. 667–674, Bristol (UK), 1998. IOP Publishing.

[GOL 85] GOLLA D. and HUGHES P., "Dynamics of viscoelastic structures – a time-domain, finite element formulation". *J. Appl. Mech.*, vol. 52, n° 4, p. 897–906, 1985.

[INM 97] INMAN D. and LAM M., "Active constrained layer damping treatments". In FERGUSON N., WOLFE H. and MEI C., Eds., *6th Int. Conf. on Recent Advances in Struct. Dyn.*, vol. 1, p. 1–20, Southampton (UK), 1997.

[JOH 81] JOHNSON C., KEINHOLZ D. and ROGERS L., "Finite element prediction of damping in beams with constrained viscoelastic layers". *Shock Vib. Bulletin*, vol. 50, n° 1, p. 71–81, 1981.

[LES 95] LESIEUTRE G. and BIANCHINI E., "Time domain modeling of linear viscoelasticity using anelastic displacement fields". *J. Vib. Acoust.*, vol. 117, n° 4, p. 424–430, 1995.

[LES 96a] LESIEUTRE G. and GOVINDSWAMY K., "Finite element modeling of frequency-dependent and temperature-dependent dynamic behavior of viscoelastic materials in simple shear". *Int. J. Solids Struct.*, vol. 33, n° 3, p. 419–432, 1996.

[LES 96b] LESIEUTRE G. and LEE U., "A finite element for beams having segmented active constrained layers with frequency-dependent viscoelastics". *Smart Mater. Struct.*, vol. 5, n° 5, p. 615–627, 1996.

[LIA 97] LIAO W. and WANG K., "On the active-passive hybrid control of structures with active constrained layer treatments". *J. Vib. Acoust.*, vol. 119, n° 4, p. 563–572, 1997.

[MCT 93] MCTAVISH D. and HUGHES P., "Modeling of linear viscoelastic space structures". *J. Vib. Acoust.*, vol. 115, p. 103–110, 1993.

[PAR 99] PARK C., INMAN D. and LAM M., "Model reduction of viscoelastic finite element models". *J. Sound Vib.*, vol. 219, n° 4, p. 619–637, 1999.

[PLO 98] PLOUIN A.-S. and BALMÈS E., "Pseudo-modal representations of large models with viscoelastic behavior". In *Int. Modal Analysis Conf.*, p. 1440–1446, Bethel (USA), 1998. SEM.

[TRI 00] TRINDADE M., BENJEDDOU A. and OHAYON R., "Parametric analysis of the vibration control of sandwich beams through shear-based piezoelectric actuation (accepted)". *J. Intell. Mater. Syst. Struct.*, 2000.

[TRI 99] TRINDADE M., BENJEDDOU A. and OHAYON R., "Amortissement hybride passif-actif des vibrations de structures composites". Rapport technique d'avancement D.G.A./D.S.P./S.T.T.C./MA. no.97-2530, Conservatoire National des Arts et Métiers, 1999.